Efficiency Trade-off-Oriented Analysis for the integration of DC-DC Converter and Battery Pack in V2G Applications

Nicola Blasuttigh
Dep. of Engineering and Architecture
University of Trieste
Trieste, Italy
nicola.blasuttigh@phd.units.it

Hamzeh Beiranvand
Chair of Power Electronics
Kiel University
Kiel, Germany
hab@tf-uni.kiel.de

Thiago Pereira
Chair of Power Electronics
Kiel University
Kiel, Germany
tp@tf-uni.kiel.de

Simone Castellan
Dep. of Engineering and Architecture
University of Trieste
Trieste, Italy
scastellan@units.it

Marco Liserre
Chair of Power Electronics
Kiel University
Kiel, Germany
ml@tf-uni.kiel.de

***Abstract*—Growing concerns about environmental aspects and clean energy generation call for effective solutions to reduce the demand for fossil fuels and greenhouse gas emissions. One solution of particular interest is the use of electric vehicles (EVs), which are considered one of the most favourable strategies for reducing pollution in the transport sector. Besides battery charging process, the EV battery pack can serve as an energy storage system (ESS) to support the grid, thanks to vehicle-to-grid (V2G) ancillary services. During the EV power exchange with the main grid, the overall efficiency depends not only on the converter but also on the battery. Typically, power converters, in particular dual-active-bridge (DAB) converters, present a low efficiency at light loads (i.e. low C-rates) and higher values at high power levels. The battery efficiency, on the other hand, decreases almost linearly as the power increases. Therefore, there is an optimum C-rate that could be selected to operate the converter and the battery when they are connected to the grid in order to minimize the losses of the overall system. In this context, the paper aims to analyze the trade-off between several designed lithium-ion battery packs and DAB efficiencies to find the best compromise. Both simulation and experimental results are presented to validate the correctness of the theoretical analyses, which also lead to an efficiency-focused design method for V2G applications.**

***Index Terms*—DC-DC converters, Efficiency, Vehicle-to-Grid, Dual Active Bridge (DAB), Lithium-ion battery**

I. Introduction

EVs are replacing the internal combustion vehicles rapidly, requiring the widespread deployment of more and more charging stations. The sale and use of electric vehicles is steadily increasing worldwide, growing from 5.1 million in 2018 to 17.5 million in 2021. This sudden spread will bring new challenges on several sides, straining the electric system to meet the related energy demand. Indeed, charging electric vehicles is currently seen as a passive load towards the grid. However, due to the ever increasing spread of smart grids and their implementation [1], electric cars will play a new role within the grid by actively behaving and exchanging energy bidirectionally. This approach is called Vehicle-to-Grid (V2G) and enables customers to exchange the stored energy of the battery pack with electric utilities as in conventional grid-connected energy storage systems [2], [3]. The system efficiency of these type of applications is crucial from the customer's point of view during battery energy exchange operations, since some of V2G applications can be remunerated [4], [5].

In this context, DAB converters are increasingly studied for bidirectional applications due to their great performance in terms of efficiency, power density and volume with the benefits of isolated systems. Moreover, interfacing of storage and DAB systems is widely explored in the existing literature [6]–[8]. DAB efficiency mainly depends on two factors: transferred power and voltage difference between the DC ports. The former causes an efficiency raise up to a maximum value after which it decreases again. The latter causes a vertical right downwards shift of the overall curve as the DC voltage mismatch increases. On the other hand, battery efficiency is very high at low C-rates, decreasing almost linearly as the C-rates increase. These two reversed trends produce a particular cross-behaviour layout which leads to a non-optimal operating power, causing higher losses either in the converter or in the battery and resulting in an undesirable condition.

Regarding the EVs future perspectives, several studies have

This work was supported in party by Gesellschaft für Energie und Klimaschutz Schleswig-Holstein (EKSH) within the framework of the project "Doppelt Schnell Doppelt Sicher (DSDS)" (Number: 8/12-39) and in part funded by the European Union - European Regional Development Fund (EFRE), the German Federal Government and the State of Schleswig-Holstein (Number: LPW-E/1.1.2/1486).

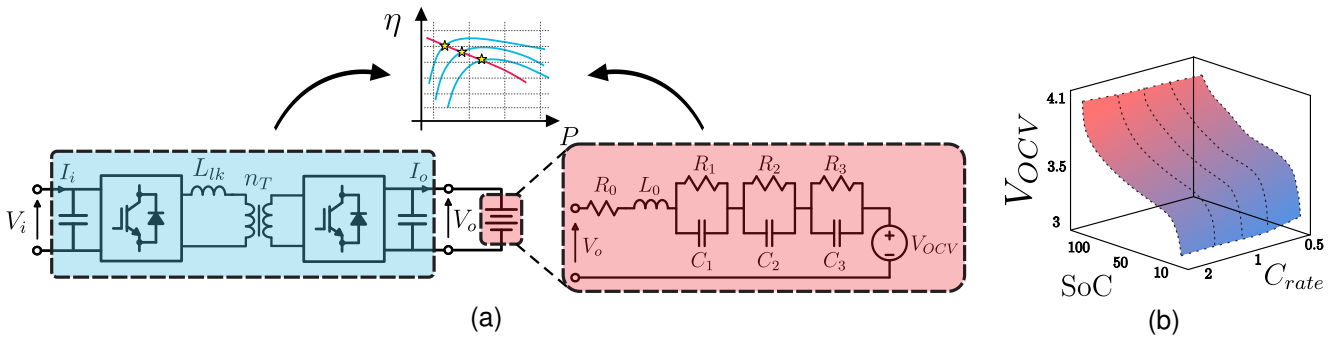

Fig. 1. a) DAB structure, battery internal model and a graphical representation of the trade-off analysis; b) Open-circuit voltage (V_{OCV}) characteristic as function of state-of-charge (SoC) and C-rate.

TABLE I
DAB CONVERTER PARAMETERS

$P_N[kW]$	$V_i[V]$	$V_o[V]$	$n_T[-]$	$L_{lk}[\mu H]$	$f_{sw}[kHz]$
20	800	600-800	1:1	61.1	20

shown that higher EV charging powers are needed to compete with internal combustion engine vehicle (ICEV) journey times. Increasing the battery pack voltage up to 800V is a possible solution to this problem, leading to considerable advantages in terms of size and weight [9]–[12]. For this reason, a trade-off analysis of single-phase DAB and battery is conducted in this paper to define the optimum compromise in terms of efficiency with these new-trend battery packs.

II. DAB AND BATTERY LOSSES ANALYSIS

A single-phase DAB connected to a battery is depicted in Fig.1a, which represents a general scheme for a potential V2G application due to its bidirectional characteristics. DAB converter is used to control the charging/discharging power of the battery, which internal model is represented in the highlighted red area. In order to obtain a comprehensive overall efficiency study, both component losses are separately analysed. First, DAB efficiency is extracted from simulations and analytical results, by implementing a single phase-shift (SPS) modulation. Then, cell losses during the entire charging/discharging process are calculated through several simulations at different C-rates considering the voltage profile over capacity. DAB parameter specifications are listed in Table I. Battery packs designs were conducted by using a 18650-format 2.8 Ah cell, which electrical model parameters are taken from [13].

A. DAB Losses Evaluation and Analysis

DAB converter losses mainly depends on semiconductor's switching and conduction behaviour, and medium-frequency transformer (MFT) losses. For the firsts, detailed simulations for the DAB under investigation are carried out providing different efficiency curves for different battery side voltages within the battery voltage range. In this way, we are able to extract only the device's losses which then will merge together with the MFT analytical losses calculations.

Although the devices losses are based on simulations, a mathematical analysis based on [14] is shown for the sake of completeness. From the analytical point of view, a general equation for conduction losses calculation for each switch can be computed as:

$$P_{S,cond} = c \cdot I_S + d \cdot I_S^2 \tag{1}$$

where I_S is the current through the device and the coefficients c, d are derived from device datasheet and curve fitting. Moreover, the coefficients can be computed as temperature-dependent if the temperature variation effect is considered.

The switching losses are more challenging to calculate, since they also depends on other surrounding parasitic components [15]. If soft-switching operations are achieved in the DAB primary side, switching losses can be neglected. Conversely, operating points outside soft-switching range can be found for the secondary side when voltage changes during the charge/discharge process of the battery pack. A good estimation of the switching losses can be described in a form:

$$P_{S,sw} = k(I_S) \cdot I_S \cdot f_{sw} = (a + b \cdot I_S + c \cdot I_S^2) \cdot I_S \cdot f_{sw} \tag{2}$$

where $k(I_S)$ is the switching-loss factor, f_{sw} is the switching frequency and the coefficients a, b and c are obtained from curve fitting calculations.

Gate drivers losses, usually neglected for the low impact on the overall performance, are also included in this study based on equations in [16]. The parasitic parameter losses such as C_{OSS} can be neglected from the calculations for frequencies around 20 kHz as considered in this work.

Further, analytical calculations are performed to obtain winding and core losses of the MFT for the same operating working points. Copper losses are computed using the well-known Dowell's equation which considers the skin and proximity effect in the transformer windings due to the high frequency waveforms behaviour. In particular, the total copper losses $P_{Cu,loss}$ can be computed as:

$$P_{Cu,loss} = I_{RMS}^2 \cdot \left(R_{ac,p} + R_{ac,s} \cdot n_T^2\right) \tag{3}$$

where I_{RMS} is the transformer RMS current for each specific operating point, $R_{ac,p}$ and $R_{ac,s}$ are the primary and secondary transformer AC resistance, respectively, and n_T is the transformer ratio. The AC primary and secondary winding

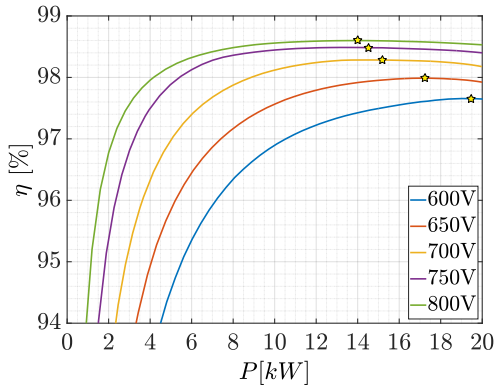

Fig. 2. Simulated efficiency curves of 20kW DAB for V_i=800V at different V_o values

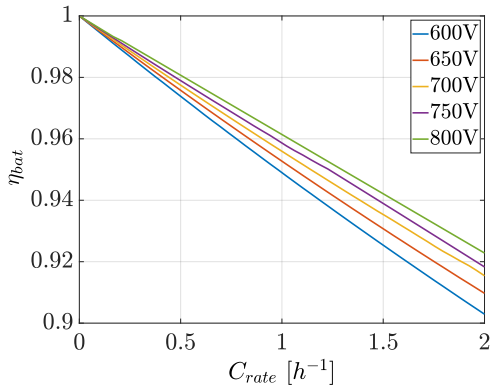

Fig. 3. Simulated efficiency curves of 20kWh battery pack for different battery voltage (i.e. SoC)

resistances are obtained through the so-called AC resistance factor [17], which is computed as:

$$F_{R_x} = R_{ac,x}/R_{dc,x} = \\ = A\left(\frac{sinh(2A)+sin(2A)}{cosh(2A)-cos(2A)}+\right. \\ \left.+\left[\frac{2(N_x^2-1)}{3}\right]\frac{sinh(A)+sin(A)}{cosh(A)-cos(A)}\right) \quad (4)$$

where $A = d_f/\delta$ is the winding conductor thickness normalised with respect to the conductor skin depth, N_x is the number of winding layers and $R_{dc,x}$ is the DC winding resistance where x denotes the primary or secondary winding.

Core losses depend on core materials and magnetic flux density within the transformer core. Since the primary and secondary voltages are non-sinusoidal, the flux density will be too, leading to the need to calculate losses with the Improved Generalized Steinmetz Equation (iGSE) [18] rather than the original Steinmetz Equation (OSE). In particular, the trapezoidal waveform of the flux density $B(t)$ during square-wave operation of the SPS modulation is considered. Under this assumption, as the phase-shift angle increases, the maximum value of the flux density B_m decreases and its derivative becomes zero within the time intervals where the primary and secondary voltage have opposite sign [19]. Considering the magnetic material properties, the core losses are calculated as:

$$P_{Core,loss} = \frac{k_i}{\pi}(2B_m)^{\beta-\alpha}\left(\frac{V_i}{2NA_c}\right)^{\alpha}\cdot \\ [\varphi|d-1|^{\alpha}+(\pi-\varphi)(d+1)^{\alpha}] \quad (5)$$

where N is the primary winding turns number, A_c is the cross section area of the core column, V_i the input voltage, $d = n_T V_o/V_i$ is the dc conversion ratio and φ the phase-shift angle. The constant parameters k_i, α and β are obtained by the core material datasheet.

A further loss contribution is due to losses in the external inductance. The calculations for this component are very similar to those used for transformer losses. Since the voltage drop across the inductance is very small and so is the resistance, the losses of this component are not considered in this work.

Figure 2 shows the simulated efficiency curves for the DAB converter at 800V primary voltage for different secondary voltages. When the two DAB's DC side voltages are at the same value, so there is no voltage mismatch, the reactive power exchange is minimal and the efficiency curve is the highest. As soon as the voltage mismatch is increased (in our case the voltage on the battery side is decreased) the reactive power exchanged increases and the efficiency curve shifts downwards due to conduction losses in the devices and in the transformer windings. Of greater interest is the shift of the points of maximum efficiency towards higher powers as the voltage mismatch increases. As it can be seen, the maximum efficiency point for $V_o = 800\,V$ is obtained for a power of about 14 kW.

Differently, for the curve at $Vo = 750\,V$ the maximum point is obtained at a power of about 14.5 kW and so on for the other voltage values. In this situation, the smaller the phase-shift angle, the greater the switching losses of the output bridge which is outside its soft-switching boundaries. In addition, even to a small extent, core losses increase towards no-load condition as it can be seen in (5). It is important to mention that these shifts in the efficiency curves and in the maximum efficiency points always exist also with lower voltage range since the effect is mainly caused by the voltage difference between the two DC ports.

B. Battery Model and Losses Evaluation

Several dynamic cell models are used and published with different complexity and accuracy. In addition to mathematical and electrochemical models, circuit-oriented models have high potential regarding precision, parametrization efforts and usability. For electric vehicle battery modelisation, different models can be found in [20], [21].

Typically, battery losses can be divided into ohmic, reversible and irreversible reaction losses. However, the terminal behavior of the battery can be described by a series of RC-pairs where the power losses can be estimated by resistances.

Several models can be used to estimate cell dynamics and characteristics in different applications. In fact, the number of poles and zeros (RC-pairs) greatly influences both the transient and the power loss estimation, which makes complicated the choice of model structure. Nevertheless, the model used in this study (Fig.1a) should be chosen for losses-calculation purposes, as presented in [13]. The battery losses are calculated by adding the Joule's losses as in (6):

$$P_{bat,loss} = P_{cell,loss} \cdot N_{tot} = R_{bat,eq} \cdot I_{bat}^2 = \\ = \sum_{j=0}^{3} R_j \cdot \frac{N_{sc}}{N_{ps}} \cdot I_{bat}^2 \tag{6}$$

where R_j is the j-th resistive element, $I_{bat} = I_o$ is the total battery current, N_{sc} is the number of series cells, N_{ps} is the number of parallel strings, $R_{bat,eq}$ is the equivalent battery pack resistance and $N_{tot} = N_{sc} \cdot N_{ps}$ is the total number of cells. Since the only measurable quantities are voltage and current at the battery terminals, the efficiency equation during charging process can be obtained as:

$$\eta_{bat} = 1 - \frac{R_{bat_{eq}} \cdot I_{bat}^2}{V_{bat} \cdot I_{bat}} = 1 - \frac{R_{bat_{eq}} \cdot I_{bat}}{V_{bat}} \tag{7}$$

where $V_{bat} = V_o$ is the DAB output voltage.

As noted, in a stationary voltage condition a linear efficiency curve is obtained. Conversely, as the voltage changes, the slope of the curves changes as shown in Fig.3. As it can be seen, in addition to the estimated value of $R_{bat_{eq}}$, the estimation of instantaneous battery efficiency depends on the measured values of voltage and current.

The internal battery pack resistance changes with several factors. The most important are temperature, SoC and the C-rate during the operations. In general, the resistance value is higher at very low temperatures and then decreases and increases again as the temperature increases as described in [22], following a quadratic function. Regarding the influence of the other factors, [23] shows typical Li-Ion internal resistance variation for different SoC and C-rate by fitting the experimental measurements as a polynomial of the third order with respect to the SoC and as an exponential function with respect to temperature. From these results, it can be said that the internal resistance increases as the SoC decreases and for SoC greater than 50% the internal resistance decreases as the C-rate growth. Further, although not treated in this work, different techniques can be used to estimate battery impedance online as a function of SoC and temperature [24]–[27].

In this study, several simulations have been performed in order to calculate battery pack losses in different voltages and C-rates working points, which are then used to obtain the total losses of the system. To this end, a cylindrical 18650-format 2.8 Ah cell is modelled by using the charge characteristic according to the most important variables, such as SOC and C-rate as shown in Fig.1b.

III. Battery Packs Design

Following the new battery voltage trend already discussed and to study the trade-off analysis in a wider battery capacity spectrum, six different batteries with the same voltage level but different capacities are designed with the 18650-format cylindrical cell under investigation. The battery pack capacities

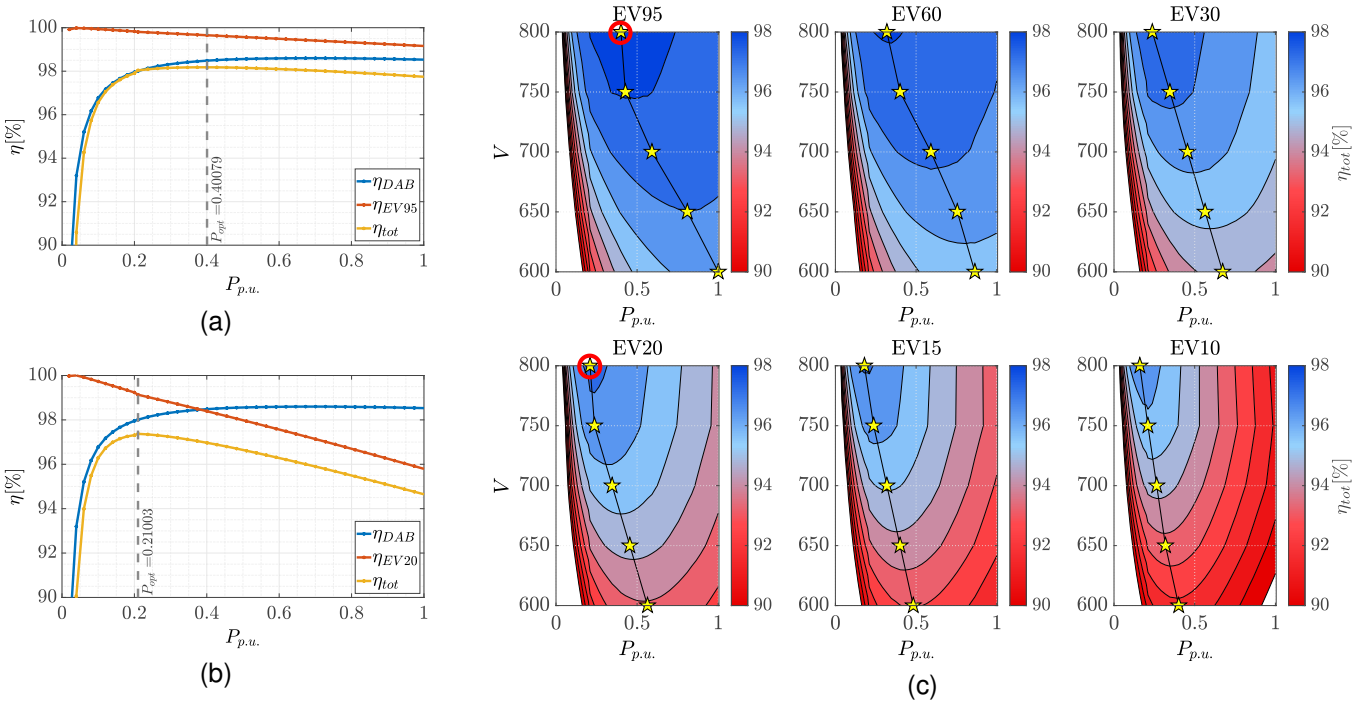

Fig. 4. a) 20 kW DAB, EV95 battery and total efficiency curves for full SoC (800V) b) 20 kW DAB, EV20 battery and total efficiency curves for full SoC (800V) c) η_{tot} efficiency values in the complete SoC range (600-800V) for different battery packs coupled with the designed 20 kW DAB: optimal points of Fig. 4a and 4b are marked with a red circle. $P_{p.u.}$ is the p.u. power referred to the DAB's nominal power.

TABLE II
800-V BATTERY PACK PARAMETERS WITH 187 SERIES CELLS AND C-RATE $_{MAX}$ = 2.

	EV95	EV60	EV30	EV20	EV15	EV10
Capacity $[Ah]$	117.6	75.6	39.2	25.2	19.6	14
N_{ps}	42	27	14	9	7	5
N_{tot}	7854	5049	2618	1683	1309	935

have been chosen related to DAB's nominal power in order to appreciate the coupling of the designed converter with different types of batteries to compare the efficiency behaviour. In particular, the idea is to compare the behaviour of the system when the capacity of the battery pack is lower (C-rate>1), equal (C-rate=1) and higher (C-rate<1) than the rated power of the DAB. The design deals with the number of cells in series and parallel to achieve battery pack specifications. A battery management system (BMS) is supposed to correctly optimise cell operation according to the relevant parameters such as temperature and voltage. In order to obtain the nominal battery voltage of 800 V, 187 series cells are used for all the battery packs, whereas the other design parameters are listed in Table II.

IV. Efficiency Trade-off Analysis

If the losses of the DAB and the battery pack are added together for the design voltage levels and for all the operating points, the total system efficiency η_{tot} is obtained. In particular, as the two systems are cascaded, the total efficiency is the product of the two efficiency curves. Figures 4a and 4b show an example of two simple trade-off cases for two different battery size at full capacity (800V): EV95 for top and EV20 for bottom figure, respectively. From the total efficiency curves the corresponding working points to achieve the overall maximum efficiency are highlighted (vertical dashed lines), showing precisely the power at which the DAB should operate to optimize the overall system losses. The first difference standing out from the comparison between the two cases is the shift in the two optimum points according to the total battery capacity (P_{opt}=0.21 and P_{opt}=0.4). This is due to the significant difference in efficiency between the two battery packs due to the lower C-rate value for the EV95. More in general, since DAB efficiency changes with the battery voltage (i.e. SoC), different total efficiency curves are obtained for a variable voltage and for each battery pack. Figure 4c shows the results of the total efficiency curves for the proposed battery packs, where each star represents a maximum efficiency point for that specific battery voltage. It is highly noticeable the difference in maximum efficiency between each battery and the shifting of the optimum power points even during the operation of a single battery. This shift is mainly due to the DAB's maximum efficiency point translation already discussed and shown in Fig.2, now even more pronounced due to the contribution of the battery efficiency curve. This approach can be used to optimize the DAB design process with respect to the maximum capacity of the battery in such a way as to design the correct sizing in a given working range and at a given efficiency range.

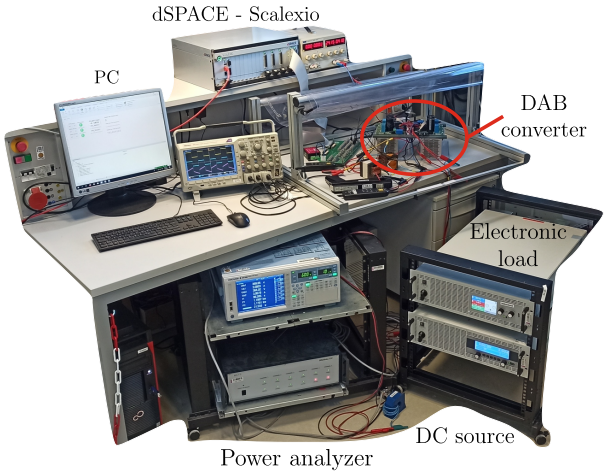

Fig. 5. The experimental setup used to validate the DAB efficiency curves.

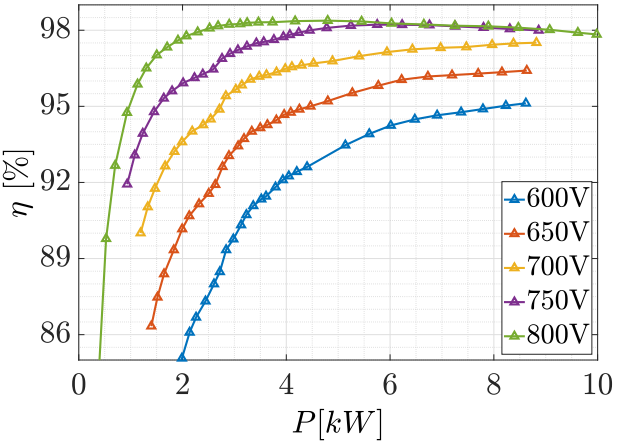

Fig. 6. Experimental efficiency measurements on 10kW DAB for $V_i = 800\,V$ at different V_o values

V. Experimental Validation

In order to validate the simulation results regarding the efficiency curves, several experiments were carried out to measure the efficiency of the DAB through the setup shown in Fig.5. The measurements are performed during the operation of a DAB with a rated power of 10 kW and a rated voltage of 800 V. The converter operates at a frequency of 20 kHz. The MFT has a ratio $n_T = 1$ and an external inductance of value $L_{lk} = 91.76\,\mu H$ is added. The SPS controller is implemented within a dSPACE Scalexio system that generates the control signals for the MOSFETs via dedicated FPGAs. All the input and output voltages and currents (i.e. V_i, V_o, I_i, I_o) are measured through a Yokogawa power analyzer which allows the calculation of the total system losses and thus the efficiency of the DAB. Primary DC voltage V_i is kept constant by a voltage DC source, whereas battery side voltage V_o is

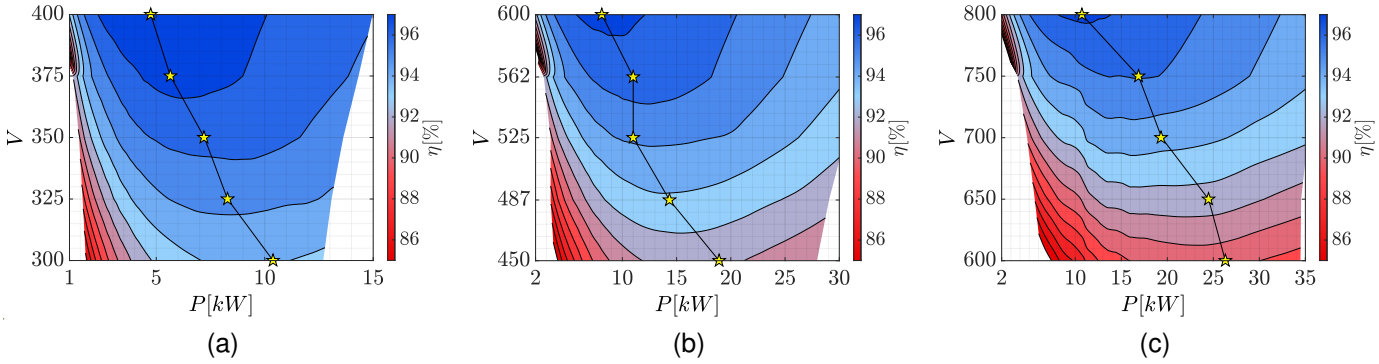

Fig. 7. Total efficiency values with four 10 kW DAB in parallel and 40 kWh battery: a) 300-400 V, b) 450-600 V, c) 600-800 V

changed by a DC load emulator within the desired battery voltage range.

Figure 6 shows the experimental efficiency curves of DAB for V_i=800V and different V_o values where a maximum efficiency of 98.4% is achieved at V_o=800V.

With the aim of evaluating DC fast-charging, a further analysis is made by considering the losses of four identical DABs connected in parallel. In contrast with the simulated tests, three different designs of 40 kWh battery packs with different voltage ranges are analysed with this parallel DAB structure. In particular, three different voltage ranges are evaluated, both for the DAB and for the battery pack: 300-400 V, 450-600 V and 600-800 V for the entire charging process. The battery losses have been calculated mathematically through the model presented in Section II-B and additively included to the measured losses of the four parallel DABs for all working points.

Figures 7a, 7b and 7c show the overall efficiency for the three voltage ranges. Due to the lower voltage range with respect to the nominal one, it can be noticed the maximum power limitation of the DAB during high-mismatch voltage operations owing to the limits on the maximum current of the MFT. However, even in this case it is possible to note the existence of an optimal trajectory that minimises the total system losses at the expense of the charging time, which in this case will be more than doubled with respect to the case in Figure 7c. Similar considerations can be extended to the cases of Figure 7b and Figure 7c where it can be seen that the increase in C-rate significantly reduces the overall efficiency of the system owing to the higher battery losses. These behaviours demonstrate the correctness of the simulations and the results discussed in Section IV.

VI. Conclusions and Future Works

The integration of charging stations into the electric grid is posing new challenges, making EV an integral and active unit of the electric system through V2G technology. The so-called "prosumers" will be given the opportunity to share energy with the grid in a bidirectional way in exchange for an economic remuneration. In this context, there may be an interest in minimising losses during the charging/discharging process. A trade-off-oriented analysis between dual-active-bridge and lithium-ion batteries efficiency curves is studied in this paper, showing that an optimal efficiency charging trajectory always exists. First, the efficiency of the DAB at different battery-side voltage levels is obtained through simulations and analytical results. Then, the efficiency of different designed lithium-ion battery packs is calculated so as to understand the behaviour of the total system efficiency. Supposing the operation of the same DAB with the proposed batteries, optimal operating points for different working conditions are shown, by highlighting the opposite behavior of the efficiency curves of the two components. In particular, optimum efficiency trajectory always exists during the charging process depending on the converter power rating versus battery capacity rating. Several experimental measurements on a 10kW DAB prototype (with a maximum of 98.4%) demonstrate the correctness of the simulation results, showing the behaviour of four DABs in parallel connected to a 40 kWh battery at different nominal voltages.

This study shows that the interface between converter and battery is a critical step from the point of view of energy efficiency. Consequently, it would be possible to develop a control that, by measuring the efficiency of the DAB and estimating the equivalent battery resistance, maximises the efficiency of the total system in real time. Future developments will be addressed towards this topic.

References

[1] M. A. Judge, A. Khan, A. Manzoor, and H. A. Khattak, "Overview of smart grid implementation: Frameworks, impact, performance and challenges," *Journal of Energy Storage*, vol. 49, May 2022.

[2] C. Betzin, H. Wolfschmidt, and M. Luther, "Electrical operation behavior and energy efficiency of battery systems in a virtual storage power plant for primary control reserve," *International Journal of Electrical Power & Energy Systems*, vol. 97, pp. 138–145, Apr. 2018.

[3] N. B. Arias, S. Hashemi, P. B. Andersen, C. Træholt, and R. Romero, "Distribution system services provided by electric vehicles: recent status, challenges, and future prospects," *IEEE Transactions on Intelligent Transportation Systems*, vol. 20, no. 12, pp. 4277–4296, 2019.

[4] E. Apostolaki-Iosifidou, P. Codani, and W. Kempton, "Measurement of power loss during electric vehicle charging and discharging," *Energy*, vol. 127, pp. 730–742, May 2017.

[5] S. Esmailirad, A. Ghiasian, and A. Rabiee, "An extended m/m/k/k queueing model to analyze the profit of a multiservice electric vehicle charging station," *IEEE Transactions on Vehicular Technology*, vol. 70, no. 4, pp. 3007–3016, 2021.

[6] A. Sharma and S. Sharma, "Review of power electronics in vehicle-to-grid systems," *Journal of Energy Storage*, vol. 21, pp. 337–361, 2019, publisher: Elsevier.

[7] M. M. Haque, P. Wolfs, S. Alahakoon, B. Sturmberg, M. Nadarajah, and F. Zare, "DAB Converter with Q Capability for BESS/EV Applications to Allow V2H/V2G Services," *IEEE Transactions on Industry Applications*, pp. 1–1, 2021, conference Name: IEEE Transactions on Industry Applications.

[8] S. Castellan, N. Blasuttigh, R. Menis, A. M. Pavan, M. Mezzarobba, and G. Buja, "Design and simulation of a vehicle-to-grid system," in *2020 6th International Conference on Electric Power and Energy Conversion Systems (EPECS)*. IEEE, 2020, pp. 69–74.

[9] I. Aghabali, J. Bauman, P. J. Kollmeyer, Y. Wang, B. Bilgin, and A. Emadi, "800-V Electric Vehicle Powertrains: Review and Analysis of Benefits, Challenges, and Future Trends," *IEEE Transactions on Transportation Electrification*, vol. 7, no. 3, pp. 927–948, Sep. 2021.

[10] A. Poorfakhraei, M. Narimani, and A. Emadi, "A Review of Multilevel Inverter Topologies in Electric Vehicles: Current Status and Future Trends," *IEEE Open Journal of Power Electronics*, vol. 2, pp. 155–170, 2021.

[11] C. Jung, "Power Up with 800-V Systems: The benefits of upgrading voltage power for battery-electric passenger vehicles," *IEEE Electrification Magazine*, vol. 5, no. 1, pp. 53–58, Mar. 2017.

[12] A. Meintz, J. Zhang, R. Vijayagopal, C. Kreutzer, S. Ahmed, I. Bloom, A. Burnham, R. B. Carlson, F. Dias, E. J. Dufek, J. Francfort, K. Hardy, A. N. Jansen, M. Keyser, A. Markel, C. Michelbacher, M. Mohanpurkar, A. Pesaran, D. Scoffield, M. Shirk, T. Stephens, and T. Tanim, "Enabling fast charging – Vehicle considerations," *Journal of Power Sources*, vol. 367, pp. 216–227, Nov. 2017.

[13] A. Kersten, "Modular Battery Systems for Electric Vehicles based on Multilevel Inverter Topologies - Opportunities and Challenges," Ph.D. dissertation, 2021.

[14] U. Drofenik and J. W. Kolar, "A General Scheme for Calculating Switching- and Conduction-Losses of Power Semiconductors in Numerical Circuit Simulations of Power Electronic Systems," in *in Proc. of the 2005 International Power Electronics Conf. (IPEC'05*, pp. 4–88 686.

[15] F. Krismer, "Modeling and optimization of bidirectional dual active bridge DC-DC converter topologies," Ph.D. dissertation, ETH Zurich, 2010.

[16] H. Beiranvand, E. Rorok, and M. Liserre, "Theoretical Evaluation of Semiconductor Loss Components Behavior in ISOP-DAB Converters," in *2019 IEEE 13th International Conference on Compatibility, Power Electronics and Power Engineering (CPE-POWERENG)*, Apr. 2019, pp. 1–7.

[17] H. Beiranvand, E. Rokrok, and M. Liserre, "*Vf* -constrained $\eta\rho$ -pareto optimisation of medium frequency transformers in ISOP-DAB converters," *IET Power Electronics*, vol. 13, no. 10, pp. 1984–1994, Aug. 2020.

[18] K. Venkatachalam, C. Sullivan, T. Abdallah, and H. Tacca, "Accurate prediction of ferrite core loss with nonsinusoidal waveforms using only Steinmetz parameters," in *2002 IEEE Workshop on Computers in Power Electronics, 2002. Proceedings.*, Jul. 2002, pp. 36–41.

[19] N. Fritz, M. Rashed, S. Bozhko, F. Cuomo, and P. Wheeler, "Analytical modelling and power density optimisation of a single phase dual active bridge for aircraft application," *The Journal of Engineering*, pp. 3671–3676, 2019.

[20] M. Chen and G. A. Rincon-Mora, "Accurate electrical battery model capable of predicting runtime and IV performance," *IEEE transactions on energy conversion*, vol. 21, no. 2, pp. 504–511, 2006, publisher: IEEE.

[21] B.-A. Enache, E. Lefter, and C. Stoica, "Comparative study for generic battery models used for electric vehicles," May 2013, pp. 1–6.

[22] Y. Chen, Y. Ma, P. Duan, and H. Chen, "Estimation of State of Charge for Lithium-ion Battery Considering Effect of Aging and Temperature," in *2018 37th Chinese Control Conference (CCC)*, Jul. 2018, pp. 8472–8477, iSSN: 1934-1768.

[23] L. Chen, M. Zhang, Y. Ding, S. Wu, Y. Li, G. Liang, H. Li, and H. Pan, "Estimation the internal resistance of lithium-ion-battery using a multi-factor dynamic internal resistance model with an error compensation strategy," *Energy Reports*, vol. 7, pp. 3050–3059, Nov. 2021.

[24] R. Koch, "On-line Electrochemical Impedance Spectroscopy for Lithium-Ion Battery Systems," Ph.D. dissertation, Technische Universität München Fakultät für Elektrotechnik und Informationstechnik, 2017.

[25] O. Theliander, A. Kersten, M. Kuder, W. Han, E. Grunditz, and T. Thiringer, "Battery Modeling and Parameter Extraction for Drive Cycle Loss Evaluation of a Modular Battery System for Vehicles Based on a Cascaded H-Bridge Multilevel Inverter," *IEEE Transactions on Industry Applications*, vol. 56, Sep. 2020.

[26] Y. Zheng, M. Ouyang, X. Han, L. Lu, and J. Li, "Investigating the error sources of the online state of charge estimation methods for lithium-ion batteries in electric vehicles," *Journal of Power Sources*, vol. 377, pp. 161–188, Feb. 2018.

[27] M. Kuipers, P. Schröer, T. Nemeth, H. Zappen, A. Blömeke, and D. U. Sauer, "An Algorithm for an Online Electrochemical Impedance Spectroscopy and Battery Parameter Estimation: Development, Verification and Validation," *Journal of Energy Storage*, vol. 30, p. 101517, Aug. 2020.